FLUID DYNAMIC VERIFICATION EXPERIMENTS ON STS-70

Final Report

NASA/ASEE Summer Faculty Fellowship Program- 1995

Johnson Space Center

Prepared By: Stanley J. Kleis, Ph.D.

Academic Rank: Associate Professor

University and Department: University of Houston
Department of Mechanical
Engineering
Houston, TX 77204-4792

NASA/JSC

Directorate: Space and Life Sciences

Division: Medical Sciences

Branch: Biomedical Operations
and Research

JSC Colleague: Neal R. Pellis, Ph.D.

Date Submitted: August 9, 1995

Contract Number: NGT-44-001-800

ABSTRACT

Fluid dynamic experiments were flown on STS-70 as phase two of the engineering evaluation of the first bioreactor Engineering Development Unit (EDU#1). The phase one experiments were comparative cell cultures in identical units on earth and onboard STS-70. In phase two, two types of fluid dynamic experiments were performed. Qualitative comparisons of the basic flow patterns were evaluated with the use of "dye" streaklines formed from alternate injections of either a mild acid or base solution into the external flow loop that was then perfused into the vessel. The presence of Bromothymol Blue in the fluid then caused color changes from yellow to blue or vice versa, indicating the basic fluid motions. This reversible change could be repeated as desired. In the absence of significant density differences in the fluid, the flow patterns in space should be the same as on earth. Video tape records of the flow patterns for a wide range of operating conditions were obtained.

The second type of fluid dynamic experiment was the quantitative evaluation of the trajectories of solid beads of various densities and sizes. The beads were introduced into the vessel and the paths recorded on video tape, with the vessel operated at various rotation rates and flow perfusion rates. Because of space limitations, the video camera was placed as close as possible to the vessel, resulting in significant optical distortion.

This report describes the analysis methods to obtain comparisons between the in-flight fluid dynamics and numerical models of the flow field. The methods include optical corrections to the video images and calculation of the bead trajectories for given operating conditions and initial bead locations.

INTRODUCTION

The bioreactor development team at NASA/JSC is responsible for the development of a complete cell cultivation system capable of growing and maintaining anchorage dependent cells in a microgravity environment for extended periods of time. The bioreactor system provides control of many parameters required for the successful cell culture while suspending the cells in a fluid environment that allows three dimensional assembly. The present report will address only the fluid dynamics within the culture vessel.

Space flight experiments in STS-70 were scheduled for June, 1995, for the bioreactor developed at NASA/JSC. Unfortunately, the flight was delayed by schedule conflicts with STS-71 and technical problems due to woodpecker damage of the external tank insulation. Two sets of experiments were scheduled; cell growth experiments and fluid dynamic verification experiments.

The current bioreactor vessel design is based in part on the viscous pump reactor vessel developed jointly by NASA/JSC and Dr. S. Kleis of the Turbulent Shear Flow Laboratory (TSFL), University of Houston [1]. The basic elements of the vessel are shown in Figure 1. A three dimensional flow field is established by rotating the outer cylinder and spin filter at different rates. Fluid enters the vessel from the external flow loop, in the gap between the left vessel end and the disc. It then circulates within the vessel before being extracted through the porous spin filter.
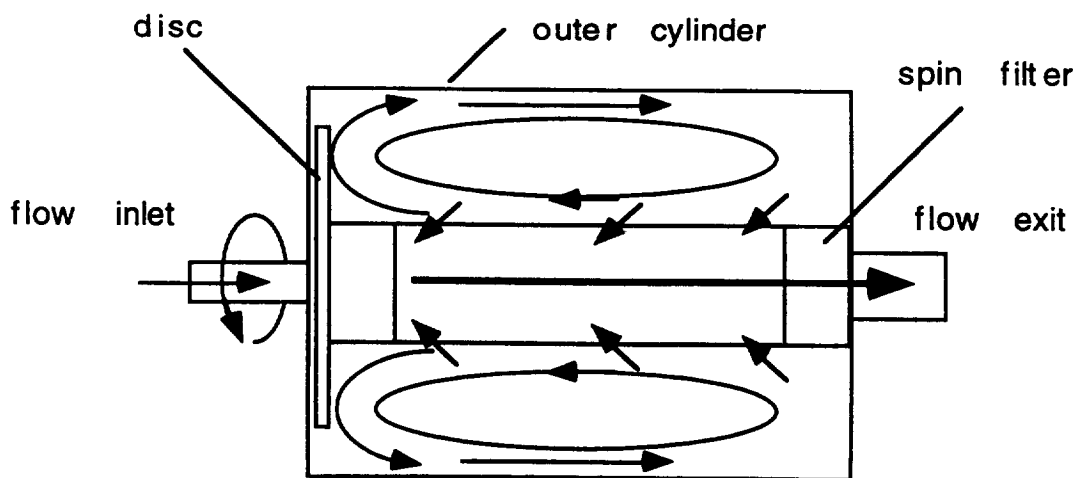

Figure 1.- EDU#1 Bioreactor Flow Fields Elements.

As part of the development of the current vessel design, a numerical model of the flow field within the vessel has been developed. The model has previously been verified under a wide range of operating conditions in a unit gravity environment by extensive measurements of the velocity fields and flow visualizations at TSFL. The purpose of the fluid dynamics phase of the flight experiments was to verify the model under microgravity conditions.

An accurate model of the fluid flow field is required to be able to predict mass transport within the vessel to be able to separate effects of changes in cell hydrodynamic environment from microgravity effects on cells. In the presence of body forces, density differences between the cells attached to micro carriers and the fluid medium cause relative motions, resulting in both mechanical shear and increased mass transport. In the microgravity environment, buoyancy effects are greatly reduced; the normal earth gravity is replaced by centripetal acceleration as the dominant body force. For a typical rotation rate of 2 rev/min in a 5 cm diameter vessel, the magnitude of the body force is reduced to approximately 0.001 m/s^2 compared with gravitational acceleration of 10 m/s^2 on earth. In the absence of other factors, cells would go from a convection dominated mass transport regime on earth to a diffusion dominated regime in microgravity. However, the viscous pump bioreactor vessel has been designed to provide a steady three dimensional flow field with controllable rates of shear. This allows the establishment of local velocity gradients. The local shear flow about the cells can provide control over the mass transfer rates. It is expected that, for most cell types, the shear rates required for adequate mass transport is well below the shear rates that causes damage to the cells by mechanical stress. In fact, it is expected that the shear rates for good mass transport are much lower than the stresses due to cells on micro carriers falling at terminal velocity in earth's gravity. If these characteristics are demonstrated, the bioreactor can be used to study the effects of controlled stress levels on cell function as well as a low stress environment for studies of direct gravity effects on cells.

The objectives of the fluid dynamic experiments conducted on STS-70 are two fold. First, flow visualizations of flow fields established under a wide range of operating conditions will be compared with similar tests previously performed at TSFL. Since

these tests are performed with nearly uniform density, the results can be compared directly with ground based experiments. The second set of fluid dynamic experiments records the positions of beads with diameters of from 1 to 3 mm moving within the bioreactor vessel. The trajectories of these particles were video taped for several different inner and outer wall rotation rates and for several perfusion rates. Unlike the flow visualization tests, these experiments will produce results that can not be obtained on earth. The results of these experiments will also be compared with the numerical model. Differences in the predicted and measured results will provide guidance for modifications to the numerical model.

OPTICAL DISTORTIONS

Conducting experiments on the mid-deck of a shuttle imposes additional constraints on the experiment design. Weight and volume limitations require careful consideration of available supplies and often change procedures. For the fluid dynamic experiments, space considerations meant mounting the video camera as close as possible to the vessel to minimize interference with the crew and other hardware (such as the main hatch, located just to the right of the EDU locker). This required the use of a 3X macro lens, which introduced additional optical distortion (the 'fish eye' effect) into the images. In addition, the bioreactor vessel itself is made of a clear polycarbonate and is filled with a cell culture medium with a refractive index near that of water. The refraction of light by the vessel acts as a cylindrical lens, distorting the apparent positions of cells and beads in the vessel. This effect was greatly reduced by placing an optical correction lens made of polycarbonate between the vessel and camera. The lens had a cylindrical surface slightly larger than the vessel on one side and a flat surface on the camera side as shown in figure 2.

The macro lens distortion can be removed from the position data if the type of distortion is known. If the lens is a simple lens, then the distortion can be approximated as a simple spherical distortion resulting from objects being different distances from the center of the lens.
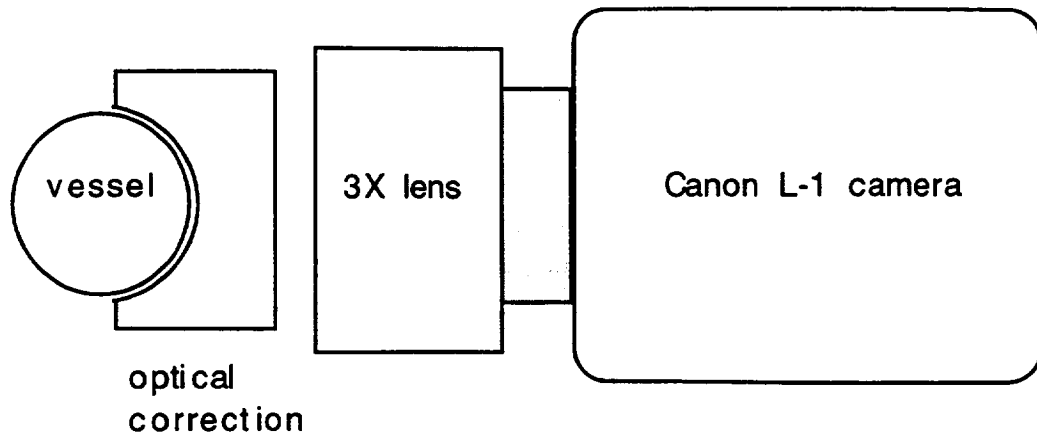
Figure 2.- Optical configure for EDU#1 videos.

For a simple 'thin' lens, the object plane distance O and the image plane distance I, are related to the lens focal length F by the relation,

$$\frac{1}{F} = \frac{1}{O} + \frac{1}{I}.$$

The height of an object in the image plane is the related to the height in the object plane by a similar relation, since

$$\frac{y_O}{O} \propto \frac{y_I}{I}.$$

Assuming that points on a spherical object plane are imaged on a flat image plane, a point at a location (x, y) on a flat object a perpendicular distance O from the lens would have a position (x', y') in the image plane, given by,

$$x' = \frac{xI}{\sqrt{O^2 + x^2 + y^2}}$$

and
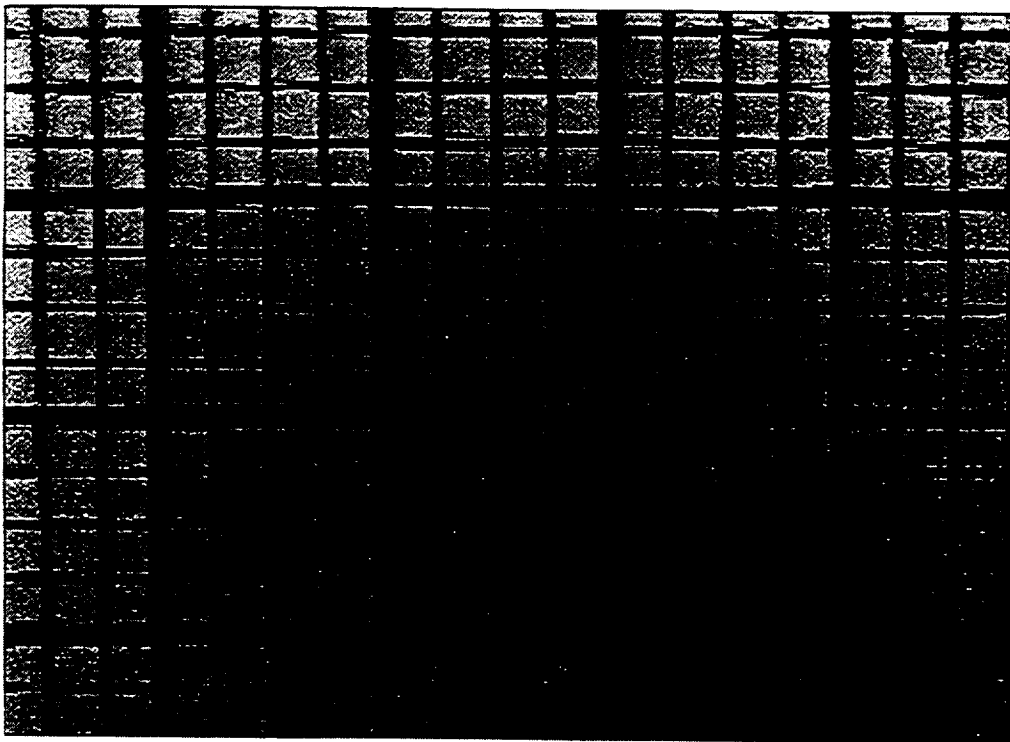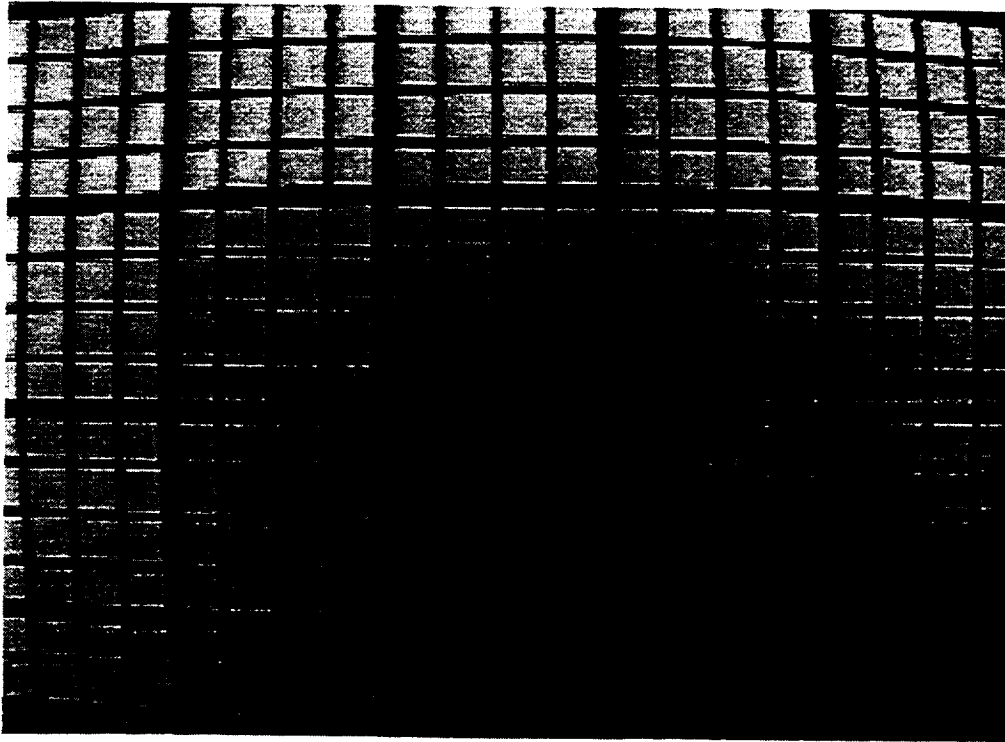
$$y' = \frac{yI}{\sqrt{O^2 + x^2 + y^2}}.$$

13-6

Figure 4.- Grid images before and after correction.

To see if this simple spherical correction would be adequate for the present study, a regular grid with lines at 0.5 in was placed in front of the flight camera at the same distance and camera settings to be used for the actual data recording. The digitized image before and after correction is shown in Figure 4. It appears that the spherical correction does a good job of removing the lens induced distortions. However, applying the correction to particle position results will require knowledge (or estimates) of the out-of-plane position of the beads. For the present study, the actual corrections will be applied to the measured positions from the original (distorted) images using estimates of the out-of-plane position of the beads. Thus, the position data will be corrected, not the images.

PARTICLE POSITION ESTIMATES

As discussed above, the relative motion between the fluid and the cells on microcarriers can have a dramatic effect on the amount of mass transport to and from the cells. In the absence of gravity or other body forces to drive convection currents, mass transport in a fluid without shear relies on diffusion. A solid sphere in a viscous flow field with shear will have a region of fluid that surrounds and moves with the sphere (a closed stream surface). When shear is present, the distance over which diffusion takes place is reduced and concentration gradients that drive the diffusion are increased. In a rotating vessel, the shear and relative motion caused by density differences in the centripetal acceleration field will determine the mass transport. Since the centripetal acceleration is about 10^4 smaller than earth's gravity, the mechanical stress on cells can be reduced to very low levels compared with those associated with the cells on microcarriers falling through the fluid in a 1 g field, by lowering the rotation rates of the spin filter and outer cylinder (see Figure 1).

The bead trajectory studies will give quantitative results that can be compared with predictions from computer models. Bead positions are estimated from force balances of the beads in the computed velocity fields for the prescribed operating conditions.

The general force balance equation for a sphere in an unsteady, non uniform flow field is [2],

$$m_p \frac{dV_i}{dt} = m_f \frac{Du_i}{Dt} - \tfrac{1}{2} m_f \frac{d}{dt} \left\{ V_i - u_i - \tfrac{1}{10} a^2 \nabla^2 u_i \right\} - 6\pi a \mu \left\{ V_i - u_i \right\} + \pi a^3 \mu \nabla^2 u_i$$

Where m_p is the mass of the particle, m_f is the mass of fluid displaced by the sphere, a is the sphere radius, V_i is the i th sphere velocity component, u_i is the corresponding fluid velocity component evaluated at the current position and time, and μ is the fluid viscosity. Note: The Basset history integral term, which accounts for the transient decay of the initial conditions, has been neglected in this equation.

When performing a force balance in cylindrical coordinates, the proper equations relating the net force to time rates of change of position are:

$$F_r = m \left(\frac{d^2 r}{dt^2} - r \left(\frac{d\theta}{dt} \right)^2 \right), \quad F_\theta = m \left(r \frac{d^2\theta}{dt^2} + 2 \frac{dr}{dt} \frac{d\theta}{dt} \right), \text{ and } F_z = m \frac{d^2 z}{dt^2}.$$

Normalizing, the resulting component equations are:

$$\left(1 + \frac{1}{2} \frac{\rho_f}{\rho_s} \right) \left(\frac{d^2 r}{dt^2} - r \left(\frac{d\theta}{dt} \right)^2 \right) =$$

$$\frac{\rho_f}{\rho_s} \frac{Du_r}{Dt} + \frac{1}{2} \frac{\rho_f}{\rho_s} \frac{d}{dt} (u_r) + \frac{a^2}{20\, r_2^{\,2}} \frac{\rho_f}{\rho_s} \frac{d}{dt} \left(\nabla^2 u_r \right) - \frac{9\mu r_2}{2 U \rho_s a^2} \left(V_r - u_r \right) + \frac{3\mu}{4 U \rho_s r_2} \left(\nabla^2 u_r \right)$$

$$\left(1 + \frac{1}{2} \frac{\rho_f}{\rho_s} \right) \left(r \frac{d^2\theta}{dt^2} + 2 \frac{dr}{dt} \frac{d\theta}{dt} \right) =$$

$$\frac{\rho_f}{\rho_s} \frac{Du_\theta}{Dt} + \frac{1}{2} \frac{\rho_f}{\rho_s} \frac{d}{dt} (u_\theta) + \frac{a^2}{20\, r_2^{\,2}} \frac{\rho_f}{\rho_s} \frac{d}{dt} \left(\nabla^2 u_\theta \right) - \frac{9\mu r_2}{2 U \rho_s a^2} \left(V_\theta - u_\theta \right) + \frac{3\mu}{4 U \rho_s r_2} \left(\nabla^2 u_\theta \right)$$

and

$$\left(1 + \frac{1}{2} \frac{\rho_f}{\rho_s} \right) \frac{d^2 z}{dt^2} =$$

$$\frac{\rho_f}{\rho_s} \frac{Du_z}{Dt} + \frac{1}{2} \frac{\rho_f}{\rho_s} \frac{d}{dt} (u_z) + \frac{a^2}{20\, r_2^{\,2}} \frac{\rho_f}{\rho_s} \frac{d}{dt} \left(\nabla^2 u_z \right) - \frac{9\mu r_2}{2 U \rho_s a^2} \left(V_z - u_z \right) + \frac{3\mu}{4 U \rho_s r_2} \left(\nabla^2 u_z \right)$$
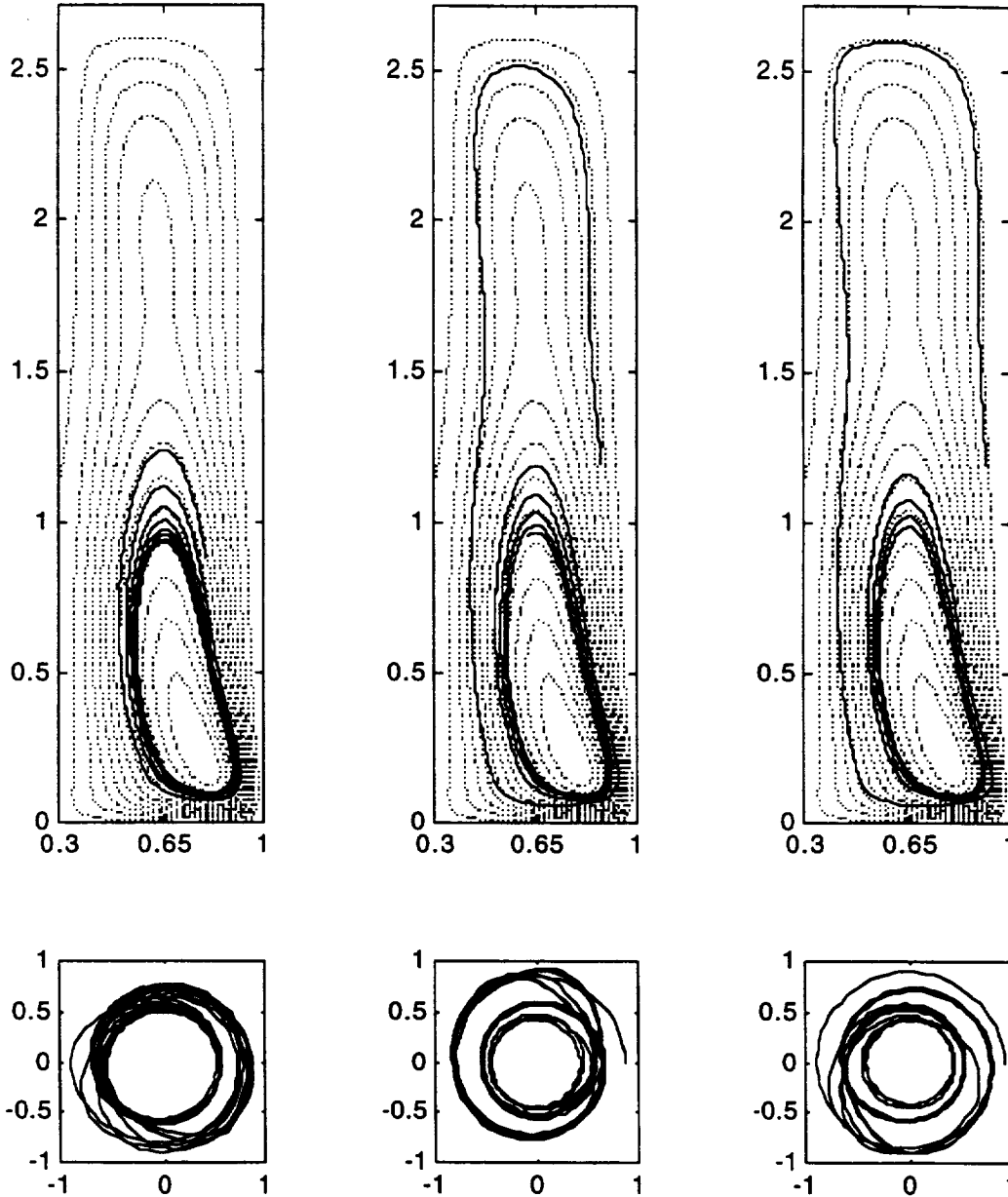
Figure 5.- Particle Trajectories for three initial particle positions (shown above figures) for the case of disc rotation rate = 11 rpm, outer cylinder rotation rate = 0.5 rpm, perfusion = 0 cc/min, bead diameter = 3.175 mm, ρ_s/ρ_f = 1.045. Total time = 5 min.

R_o=2 cm, Z_o=2 cm R_o=2.3 cm, Z_o=3 cm R_o=1.875 cm, Z_o=1.875 cm
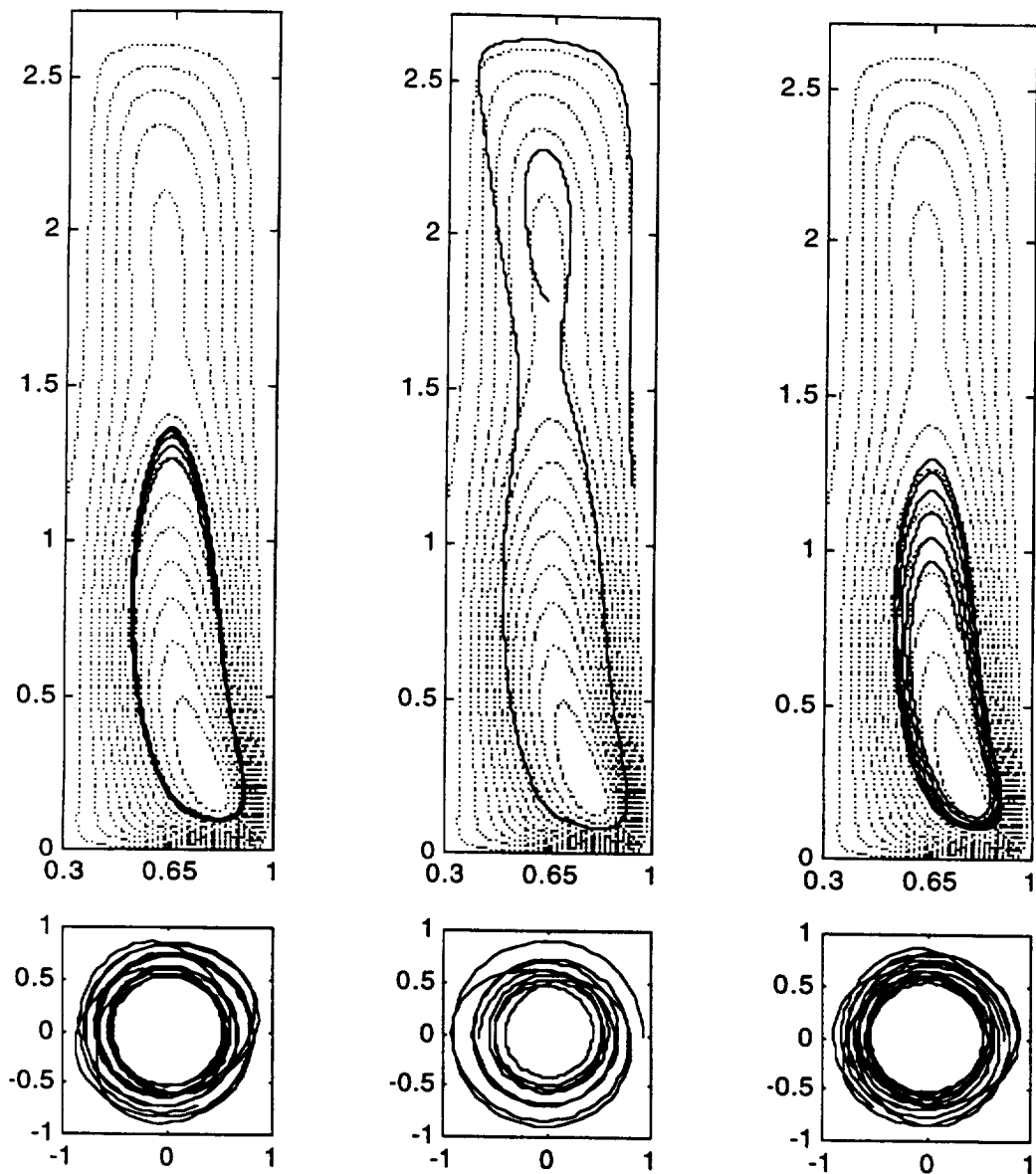

Figure 6.- Heavier particle trajectories for three initial particle positions (shown above figures) for the case of disc rotation rate = 11 rpm, outer cylinder rotation rate = 0.5 rpm, perfusion = 0 cc/min, bead diameter = 3.175 mm, ρ_s/ρ_f = 1.18. Total time = 5 min.

$R_o=2$ cm, $Z_o=3.75$ cm $R_o=1.8$ cm, $Z_o=1.5$ cm $R_o=2$ cm, $Z_o=2$ cm
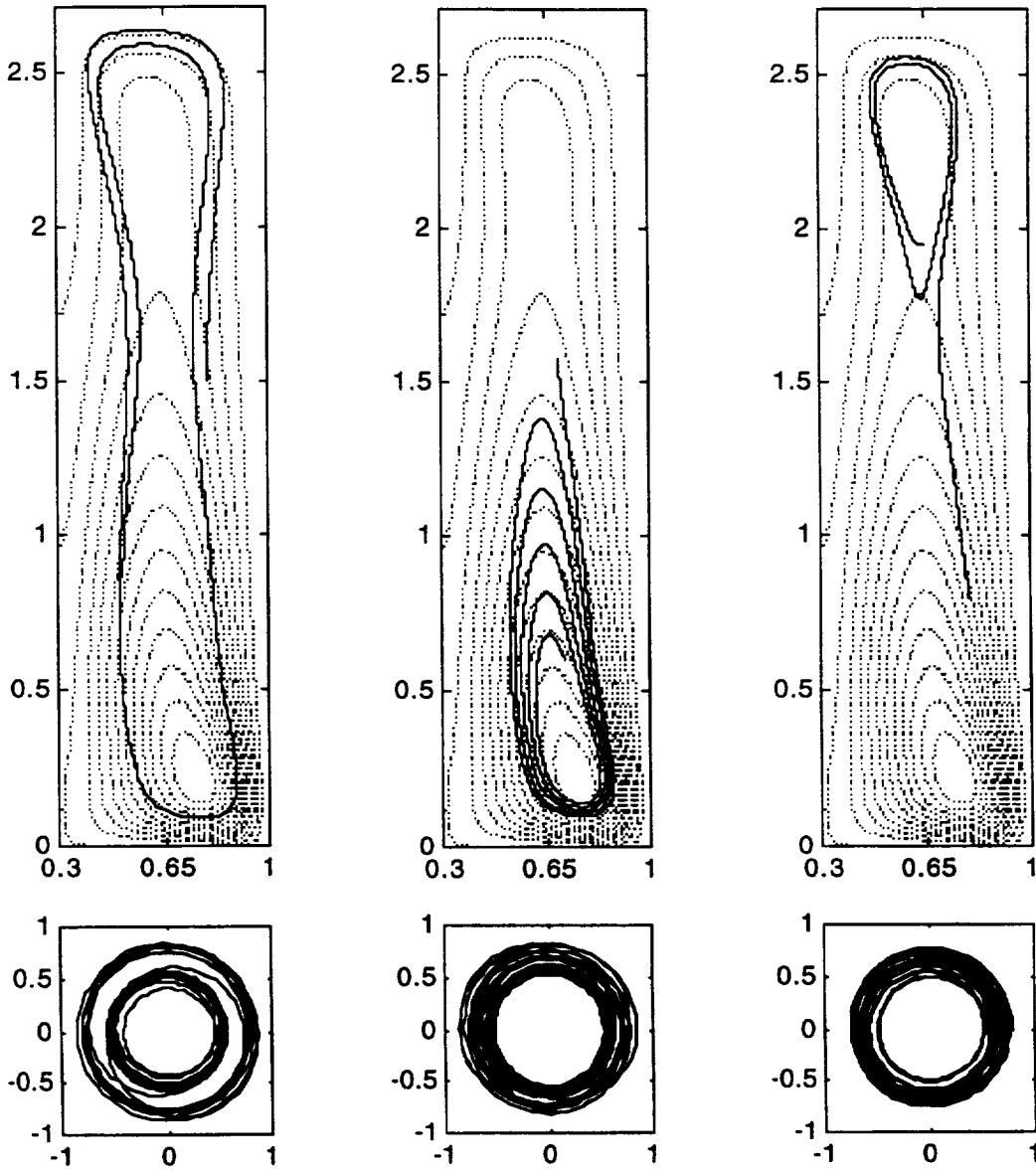

Figure 7.-   Heavier particle trajectories for three initial particle positions for the case of disc rotation rate = 6 rpm, outer cylinder rotation rate = 1.0 rpm, perfusion = 10 cc/min, bead diameter = 3.175 mm, ρ_s/ρ_f = 1.18.   Total time = 10 min.
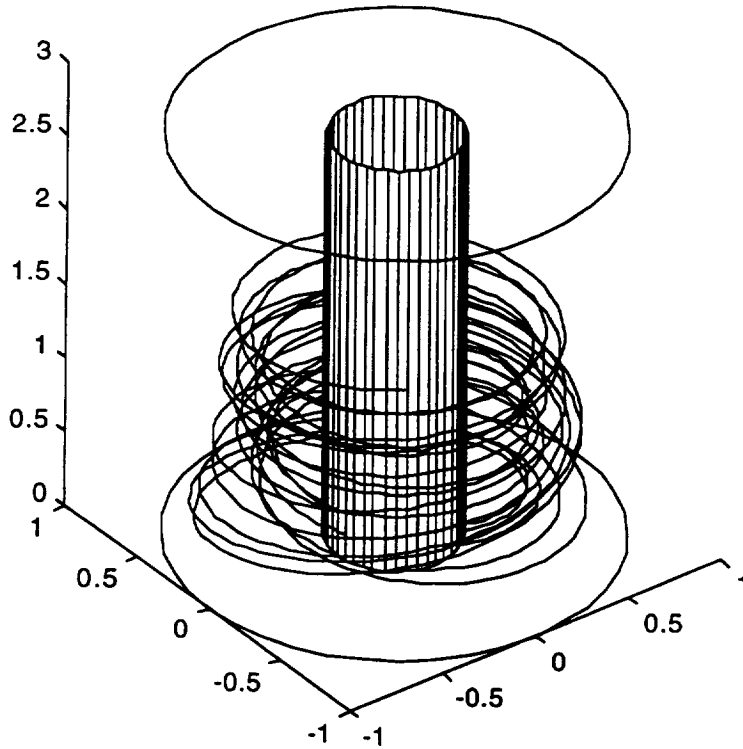
Figure 8.- Heavier particle trajectory for initial particle position (1.8 cm, 0, 1.5 cm) for the case of disc rotation rate = 6 rpm, outer cylinder rotation rate = 1.0 rpm, perfusion = 10 cc/min, bead diameter = 3.175 mm, ρ_s/ρ_f = 1.18. Total time = 10 min.

In these equations the fluid and sphere velocities have been normalized by the characteristic velocity, U, the larger of the tip velocity of the disc or outer cylinder, and the length scale used was r2, the radius of the outer cylinder of the bioreactor (2.5 cm for the current design). The subscripts s and f refer to the sphere or fluid, respectively.

These equations were solved using a forth order Runga-Kutta method for the position coordinates as functions of time using the fluid velocities computed by a previous numerical model for steady fluid motion. Figures 5, 6, and 7 show the bead trajectories in side

views, (r, z) planes, in the top figures and top views, (r, θ) planes, in the lower figures. In each figure, three initial bead positions are shown. Figure 5 represents the conditions used for the cell experiments on STS-70, with a bead density ratio near that of cells on microcarriers. Figure 6 is for the same operating conditions, but for a bead whose density ratio and size match the bead used in the fluid dynamic experiments of STS-70. Figure 7 is for a lower rotation rate, typical of future cell studies. In all cases, the bead is suspended in the fluid (stays off the outer wall) with significant axial and radial motions. Figure 8 shows a perspective view of the three dimensional bead motion.

It is interesting to note that the equations of motion show that neutrally buoyant larger beads in a general three dimensional flow field will not follow the streamlines. The terms including the Laplacian of the fluid velocity do not approach zero as the bead density approaches that of the fluid. Thus, a zero relative velocity is not a solution for neutrally buoyant bead. These terms do approach zero in the limit of small bead size. This is a reflection of the differences between a rigid sphere and a deformable fluid element.

Several test cases have been used to verify the accuracy of the bead position calculations. These include flow fields for solid body rotation and simple Couette flow with infinitely long cylinders. The results agreed as expected. Unfortunately, there is no known exact solution which has all three velocity components. The predictions do, however, behave properly (follow streamlines) for the case of small beads in a computed three dimensional flow.

CONCLUSIONS

It has been shown that a simple spherical optical correction for the macro lens is adequate for processing bead position data. Estimates of the out-of-plane coordinate will be necessary to process the bead position results from STS-70.

Bead position predictions based upon previous numerical models of the flow field and force balances on the beads have been developed for comparison with the flight experiments. The flight experiment video tapes have just become available. However, preliminary results indicate that the predicted trajectories look qualitatively similar to the bead trajectories observed in the down

linked videos from the flight experiments. More quantitative comparisons are being made.

REFERENCES

1. "A Viscous Pump Bioreactor," S. Kleis, S. Schreck, and R. Nerem, Biotechnology and Bioengineering, Vol. 36, pp. 771-777 (1990).

2. "Equation of Motion for a Small Rigid Sphere in a Nonuniform Flow," M. R. Maxey and J. J. Riley, Phys. Fluids, **26**, pp. 883-889, (1983).